POLITECNICO DI TORINO
Repository ISTITUZIONALE

Electrochemical and impedance characterization of Microbial Fuel Cells based on 2D and 3D anodic electrodes working with seawater microorganisms under continuous operation

(Article begins on next page)

23 December 2024

Electrochemical and impedance characterization of Microbial Fuel Cells based on 2D and 3D anodic electrodes working with seawater microorganisms under continuous operation

D. Hidalgo [a,b], A. Sacco [a], S. Hernández [a,b], T. Tommasi [a,*]

[a] Center for Space Human Robotics @PoliTO, Istituto Italiano di Tecnologia, C.so Trento 21, 10129 Torino, Italy
[b] Applied Science and Technology Department, Politecnico di Torino, C.so Duca degli Abruzzi 24, 10129 Torino, Italy

GRAPHICAL ABSTRACT

Electrochemical and Impedance characterization of Microbial Fuel Cells based on 2D and 3D anodic electrodes working with seawater microorganisms under continuous operation
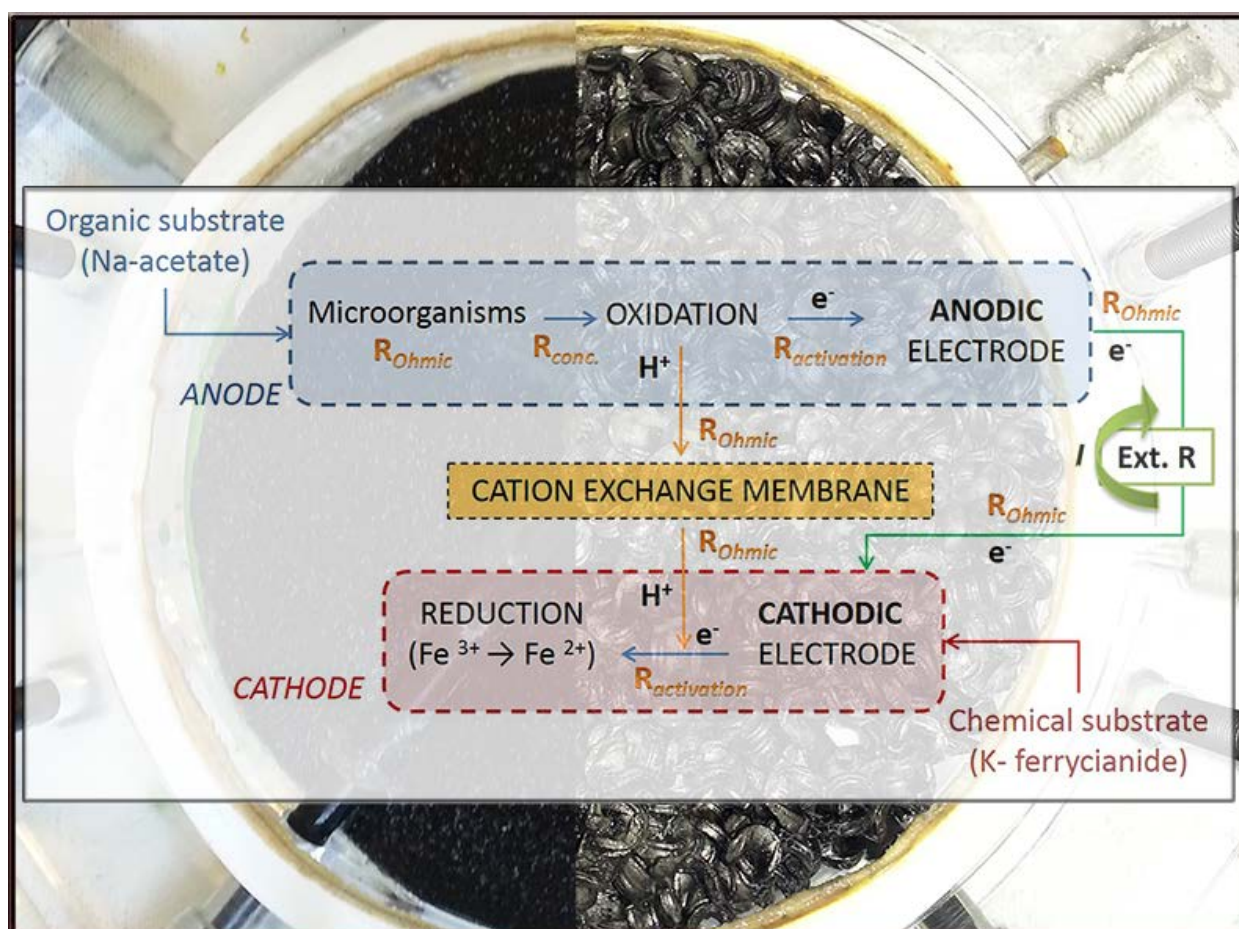
D. Hidalgo [a,b], A. Sacco [a], S. Hernández [a,b], T. Tommasi [a,*]

a Center for Space Human Robotics @PoliTO, Istituto Italiano di Tecnologia,
C.so Trento 21, 10129 Torino, Italy.
bApplied Science and Technology Department, Politecnico di Torino,
C.so Duca degli Abruzzi 24, 10129 Torino, Italy.
*Corresponding author:
e-mail: tonia.tommasi@iit.it, Tel . : +390110903414; Fax :+390110903401

Abstract

A mixed microbial population naturally presents in seawater was used as active anodic biofilm of two Microbial Fuel Cells (MFCs), employing either a 2D commercial carbon felt or 3D carbon-coated Berl saddles as anode electrodes, with the aim to compare their electrochemical behavior under continuous operation. After an initial increase of the maximum power density, the felt-based cell reduced its performance at 5 months (from 7 to 4 $\mu W \cdot cm^{-2}$), while the saddle-based MFC exceeds 9 $\mu W \cdot cm^{-2}$ (after 2 months) and maintained such performance for all the tests. Electrochemical impedance spectroscopy was used to identify the MFCs controlling losses and indicates that the mass-transport limitations at the biofilm-electrolyte interface have the main contribution (> 95 %) to their internal resistance. The activation resistance was one order of magnitude lower with the Berl saddles than with carbon felt, suggesting an enhanced charge-transfer in the high surface-area 3D electrode, due to an increase in bacteria population growth.

Keywords: Microbial Fuel Cell, Electrochemical Impedance Spectroscopy, 3D electrode, carbon-coated Berl saddles, enriched seawater inoculum

1. Introduction

Microbial Fuel Cells (MFCs) are devices that use microorganisms like bacteria to oxidize organic and inorganic matters and generate electricity, thus potentially having a dual function (*i.e.* wastewater treatment and energy production). A typical MFC consists of anode and cathode chambers separated by a Cation Exchange Membrane (CEM). Microbes in the anodic chamber oxidize added substrates and generate electrons and protons during this process (Du et al., 2007). The electrons generated are captured by the anode electrode material and then transferred to the cathode via an external circuit, which results in the generation of electricity under an external load (resistor) (Arends et al., 2012; Logan et al., 2006). After crossing the CEM, the protons arrive in the cathodic chamber, in which the reduction reaction takes place. Electric current generation is made possible by keeping microbes separated from oxygen or any other end-terminal acceptor other than the anode, which requires anaerobic conditions.

Microorganisms contained in different natural environments such as marine water and sediments, wastewater and soils can be used as active bacteria at the anode chamber of an MFC. During the device operation, planktonic population into the liquid and biofilm on the electrode surface grow after the initial inoculation. Nevertheless, the biofilm need to adapt to the MFC environment, which can take from about 4 days up to more than

100 days in order to establish a mature biofilm (Yu et al., 2012).

Some fundamental questions attracting attention are how microbes transport electrons through a thick biofilm and across the biofilm/anode interface, and which are the main resistances involved on that process (Bond et al., 2012). Figure 1 shows an overview of the main processes involved in the whole MFC operation, related to each reaction (e.g. oxidation and reduction) in the two different compartments and to the charges (electrons and cations) migration between anode and cathode through both the CEM and the external electrical circuit, respectively. First, microorganisms are employed as catalyst in the anode chamber for the metabolism reactions of the organic substrate (e.g. acetate oxidation) that is decomposed into protons, electrons and metabolites. The electrons present into extracellular environment are released and transferred to the electrode surface, by either carriers or direct contact of outer bacteria membrane or pili with the electrode surface. Hence, electrons travel through the external circuit to the cathode globally producing electricity. Concomitantly to acetate oxidation, protons are generated; they diffuse through the anolyte and then through the CEM, reaching the cathode compartment. The protons and electrons react on the cathode surface with an electron acceptor.

The different processes and resistances schematized in Figure 1 are detailed in the following.
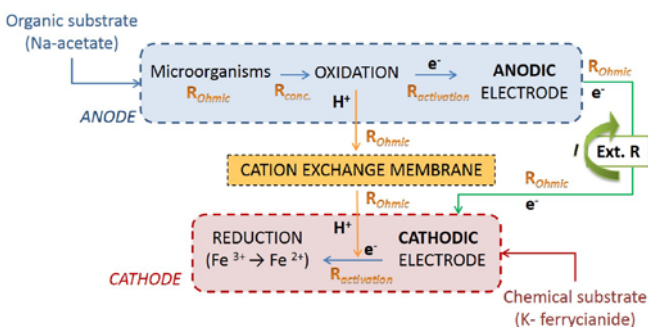
Figure 1. Schematic view of a Microbial Fuel cell, with the indication of the resistances contributing to the total internal resistance of the system. R_{Ohmic}: Ohmic resistance; $R_{conc.}$: concentration resistance; $R_{activation}$: activation resistance.

Activation resistance ($R_{activation}$), also called charge-transfer resistance, depends on catalysts, electrochemical mediators, biofilm, microbial species and their metabolisms, and operative conditions such as temperature and pH. It derives from the slowness and irreversibility of the reactions taking place on the surface of the electrodes (Zhao et al., 2009). Ohmic resistances (indicated as R_{Ohmic}) are mainly caused by ionic resistances of electrolyte, membrane and biofilm, and by electronic resistances of electrodes, current collectors and electrical connections (Zhao et al., 2009). Concentration or mass-transfer limited polarization resistance ($R_{conc.}$) mainly depends on the rate of electrons and protons diffusion, required to sustain the generation of current. Mass-transfer resistances are affected by geometry of the cell, electrolytes, structure of the electrodes and biofilm, metabolites and products.

In this work, the performance of an MFC with a three-dimensional (3D) electrode in the anode chamber has been investigated in comparison with such of an MFC containing a bi-dimensional (2D) one, with the aim to understand the influence of such electrode materials on both biofilm formation process and electrochemical activity of a mixed consortia obtained from seawater, under realistic operative conditions (*i.e.* continuous operation mode during 5 months). In particular, the improved behavior of innovative 3D carbon-coated Berl saddles (specific surface area 0.5 $m^2 \cdot g^{-1}$), recently developed in our laboratories (Hidalgo et al., 2014), has been compared with such of a reference 2D commercial carbon felt material (specific surface area 1.5 $m^2 \cdot g^{-1}$). Packed-structures, as Berl saddles, are becoming increasingly common in MFCs since they provide high surface area available to bacteria (Aelterman et al., 2008; Di Lorenzo et al., 2010). In addition to polarization curves to study the MFCs electrochemical properties, the dynamic of charge-transport and transfer processes in both the systems have been in-depth studied by Electrochemical Impedance Spectroscopy (EIS) analysis. Indeed, polarization curves are generally

used to measure the open circuit voltage (OCV) and to estimate both the maximum current density and the maximum power output of the MFCs (Clauwaert et al., 2008). Instead, EIS is a powerful AC technique widely employed in different fields of electrochemistry (Barsoukov & Macdonald, 2005; Hernández et al., 2014; Hernández et al., 2015), including MFC systems (Dominguez-Benetton et al., 2012; Martin et al., 2013; Sanchez-Herrera et al., 2014), which results highly useful when the different resistances values for each process involved in the MFC operation cannot be easily determined from a polarization curve. EIS is considered as an accurate technique for analyzing bio-electrochemical reactions on electrodes, internal resistances, biofilm development and immobilization on the different materials, estimating electrode properties, and studying the mass transfer resistances due to the diffusion limitations of the reactants (Dominguez-Benetton et al., 2012; He & Mansfeld, 2009; Manohar et al., 2008). On the contrary, the most commonly used current interrupt method precludes the differentiation of the non-ohmic effects of the charge-transfer resistance at the electrochemical interface (both anode and cathode), the electrochemical double layer capacitance at the electrodes, and the mass transfer processes (Logan et al., 2006). Hence, EIS has been used in order to understand the principal phenomena playing a positive role or limiting the electrical energy generation in the here proposed innovative MFC system, looking forward to have insights on the development of optimized materials that generate high electrical power densities (Dominguez-Benetton et al., 2012).

2. Experimental

2.1. Materials

Commercial carbon felt (C-FELT) (Soft felt SIGRATHERM GFA 5, SGL Carbon, Germany) and carbon-coated Berl saddles (C-SADDLES) were used as anode electrodes. The C-SADDLES were obtained from commercial Berl saddles following these consecutive steps: (a)

impregnation in α-D-glucose solution (500 $g \cdot L^{-1}$) for 24 h, (b) caramelization at 185 °C under vacuum for 24 h and (c) pyrolysis at 800 °C under N_2 flux (500 $mL \cdot min^{-1}$) for 2 h and then let to cool down overnight. More details regarding to C-SADDLES synthesis procedure can be found in (Hidalgo et al., 2014). All experiments were conducted using C-FELT in the cathode chamber. Sodium acetate ($\geq$ 99%), peptone (bacteriological for microbiology), potassium ferricyanide ($\geq$ 99%), sodium phosphate dibasic dihydrate ($\geq$ 98%) and sodium phosphate monobasic monohydrate ($\geq$ 98%) were used as purchased from Sigma Aldrich to conduct the electrochemical experiments in the MFCs.

2.2. Bacterial growth conditions

The fresh seawater sample (from Arma di Taggia, Imperia, Italy), before to be used as inoculum in MFCs, was previously enriched under anaerobic condition in 250 mL glass flasks in a three steps process. In the first step, the fresh seawater was inoculated (10 % *v/v*) into a synthetic substrate, with the following composition in $g \cdot L^{-1}$: 7 $C_6H_{12}O_6$, 8.2 Na_2HPO_4, 5.2 NaH_2PO_4, 8 CH_3CO_2Na, 7 fructose and 10 peptone. These reagents were dissolved in 75 % *v/v* filtered seawater and 25 % *v/v* distilled water. After that, the pH of culture was set-up in the range 7 - 7.5 by adding 2 N NaOH. In order to reach strictly anaerobic condition, each culture was purged by N_2 flow for 5 min. The "culture enrichment" was conducted at room temperature (24 ± 2 °C) under gentle orbital shaking (150 rpm). The bacteria growth was monitored by measuring the optical density with a UV–visible spectrophotometer (PerkinElmer, Lambda 35, USA) at 600 nm (OD_{600}) of liquid samples over the time. When the OD_{600} was in the range 0.5 - 0.8 (*i.e.* corresponding to the exponential phase of bacteria growth), 10 % culture was used as inoculum for the new fresh culture (second step), which contains the same medium described before and the same operative conditions. Once again, when the culture reached an OD_{600} in the range

0.5 - 0.8, it was inoculated in the third fresh medium, repeating the same procedure. When the OD_{600} was in the range 0.5 - 0.8, the inoculum was ready to be inoculated into the anodic chamber of the MFC for the tests, in a concentration of 10 % *v/v* with respect to the total anode volume.

2.3. MFC configuration and operation

Each MFC consists of two circular chambers, *i.e.* the anode and the cathode. Both compartments were made in Poly(methyl methacrylate), with dimensions equal to 12 cm (diameter) and 1.5 cm (width), separated by a CEM (CMI 7000, Membranes International Inc.) as shown in Figure S1 of the Supporting Information (SI). The total liquid volume of each chamber was around 170 mL. Experiments were conducted in two identical MFCs with the same operational conditions. The first cell was operated using the C-FELT and the second cell was operated using the C-SADDLES. All experiments were conducted using C-FELT as cathode electrode material. The conductive materials were introduced into each chamber and connected with a graphite rod (diameter 5 mm), to ensure an effective current transport to the external electrical circuit. The two MFCs were operated in a continuous mode with an external resistance of 1 kΩ during more than 5 months of operation at room temperature, with the exception of the first 3 days, during which the cells were maintained under OCV conditions, *i.e.* without external load.

The MFCs were inoculated with the effluent of an active MFC previously enriched as described in Section 2.2. The anolyte consisted of the inoculum (50 mL), sodium acetate (1 g·L^{-1}) and peptone (1.25 g·L^{-1}) in a bufferred solution composed of 30 % *v/v* of fresh seawater and 70 % *v/v* of inorganic salts (buffer), *i.e.* $Na_2HPO_4 \cdot 2H_2O$ (8.2 g·L^{-1}) and $NaH_2PO_4 \cdot H_2O$ (5.2 g·L^{-1}). The total volume of the anolyte was 500 mL, which was recirculated from an external anode vessel through the anode chamber at a flow rate of 1 L·h^{-1} by a peristaltic pump (ISMATEC -

ISM404B, Germany). A N_2 flow was used to ensure anaerobic conditions in the anode chamber at the beginning of the experiment.

A synthetic anode influent was also continuously fed by a syringe pump (NE-1600 Programmable Syringe Pump, New Era Pump Systems, USA) at a flow rate of 0.42 mL·h^{-1}, in order to provide to each anodic chamber of the MFCs 1 g·L^{-1} of sodium acetate and 1.25 g·L^{-1} of peptone per day, with respect to the total volume of the anolyte. During the experiments, the total anolyte volume was maintained at 500 mL by using a vessel system for the collection of the exceeding anolyte solution.

The catholyte consisted of a potassium ferricyanide (500 mL at 6.58 g·L^{-1}) aqueous solution in a buffer solution of inorganic salts (phosphate buffer), with the same concentration as described above. This solution was recirculated from the cathode vessel through the cathode chamber at a flow rate of 1 L·h^{-1} by using a multichannel peristaltic pump (Peri-Star Pro Peristaltic Pump, World Precision Instrument, USA). The reduction happening into the cathode chamber was controlled by a periodic renewal of the catholyte when the solution was decolorized.

2.4. Electrochemical measurements and energy production using MFC

Electrochemical experiments were performed using a multi-channel VSP potentiostat/galvanostat (BioLogic, France). Measurements were recorded by using EC-Lab software version 10.1x for data acquisition. All tests were carried out using a two-electrode configuration, where the working electrode was coupled to the anode and both counter and reference electrodes were connected to the cathode. The polarization curves were recorded through the Linear Sweep Voltammetry (LSV) technique by imposing a linear potential decrease from the OCV ($I = 0$) to the short circuit (SC) (where $I = I_{max}$) of the cell, at a scan rate of 1 mV·s^{-1}. From such *I-V* curves, the power density was calculated by using the following equation: *P*

= $(I \cdot V) \cdot A^{-1}$, where I, V and A represent the recorded current, the voltage output and the total area of the chamber, respectively.

EIS measurements were carried out through a VSP potentiostat, using both two-electrode (as described above) and three-electrode configurations. In the latter case, the anodic and cathodic chambers were analyzed individually. To this purpose, the anode (or the cathode) was used as working electrode, the cathode (or the anode) was used as counter electrode, and an Ag/AgCl electrode was used as reference, by inserting it into the anodic (or cathodic) chamber, respectively. For all the EIS measurements, the amplitude of the alternating current signal was 25 mV, and the frequency range was $10^{-2} – 10^5$ Hz. The two-electrode measurements were performed in open circuit condition, and the three-electrode ones by varying the applied bias voltage from OCV to SC.

3. Results and discussion

3.1. Long-term evaluation test in two-electrode configuration

#### 3.1.1. Polarization curves and power generation

Figure 2 shows the polarization and power density curves of both C-FELT and C-SADDLES based MFCs. The initial performances (at 0 days: corresponding to about 2 h of operation) of both MFCs were extremely low as expected, due to the almost absence of metabolic bacteria activity. Hence, OCV conditions were maintained during the first 3 days of operation in order to reach a stable potential and to favor the bacteria adaptation, without the stress induced by any external resistance. The lag-phase of bacteria growth lasts about 48 hours, as was confirmed by monitoring the planktonic absorbance of the anode electrolytes. After that period, there was an exponential phase of growth, concomitantly with an increase of voltage. Therefore, after such time (72 hour), an external resistance equal to 1 kΩ was applied between anode and cathode electrodes, and the voltage was continuously monitored.

At first glance of Figure 2a and 2c, it is possible to note the different behaviors of LSV curves of the C-FELT and C-SADDLES based MFCs, respectively. The C-FELT MFC shows a more sweeping decrease of voltage when the current increases with respect to the C-SADDLES cell. The sudden lowering of voltage affects the power density curve of the C-FELT cell, with very visible and sharp peaks (see Figure 2b). Such behavior reveals the instability and difficulty to maintain the maximum power point (MPP) of the system operating under realistic continuous conditions; indeed, if the voltage or the current move from such MPP, the power drop will be remarkable. In contrast, the C-SADDLES MFC evidences more stable MPP conditions (see Figure 2d), giving a better performance in a broader range of I-V values.

Focusing on the time-course of the tests in Figure 2, the LSVs and consequently the cells performances roughly increase over time for both MFCs. However, after 5 months the C-FELT cell suffered a decrease of the MPP (from 7 to 4.2 $\mu W \cdot cm^{-2}$). Instead, for the C-SADDLES MFC, the MPP exceeds 9 $\mu W \cdot cm^{-2}$ after 2 months (60 days) and such condition was maintained even after 5 months of continuous operation. Both the MFCs have an atypical shape of the LSV curves that is recurring over time. In the case of the C-FELT, it presents three inflection points and different slopes in the curves. Instead, for the C-SADDLES the behavior seems constant in a straight line from OCV until SC conditions. This makes difficult the comprehension of the three diverse regions corresponding to the different resistance components that contribute to the total energy losses. In general, different slopes in the LSV curve can be correlated with different contributions to the internal resistance: the activation or charge-transfer resistances (near to OCV), and the concentration or mass-transfer limited resistance (near to SC), both constituting
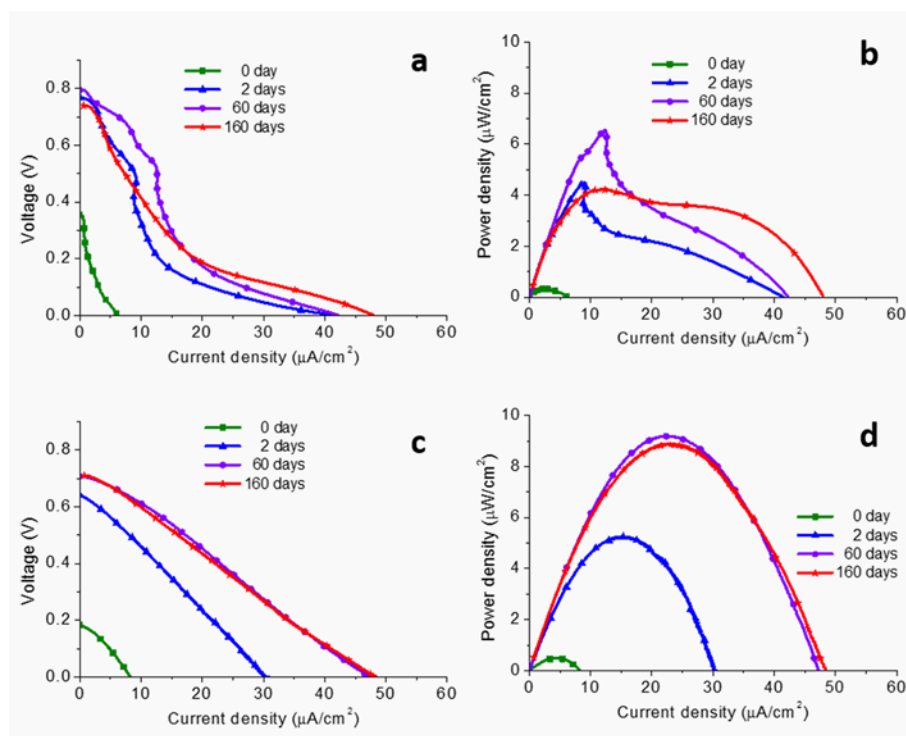
Figure 2. (a and c) Polarization (*I-V*) and (b and d) corresponding power density curves for: carbon felt-based (a and b) and Berl saddles-based (c and d) MFCs, during the time-course of the tests.

the polarization resistance of the (bio)electrodes; and the ohmic resistance, in the middle section of LSV (Dominguez-Benetton et al., 2012; Manohar & Mansfeld, 2009).

3.1.2. Optical density study

Moreover, optical density analysis (OD_{600}) of 1:5 diluted samples reveals a constant growth of the microorganisms in the liquid anolyte with increasing operation time, showing average absorbance values of 0.6 and 0.8, for the C-FELT and C-SADDLES MFCs, respectively. In the Berl saddles-based cell, the larger value of absorbance can be related to a higher and well-distributed biofilm inside the cell. Indeed, there was not a significant change in the OD_{600} on this cell after the first 2 days (lag-phase (Tommasi et al., 2008)). Instead, for the carbon felt-based MFC, a slightly decreases of the OD_{600} has been noticed, which suggest a non-uniform distribution and growth of the bacteria population in this anodic material. Despite the fact that this analysis is representative of planktonic population living in the liquid

solution, these results also allow to have an indication of the biofilm formation on the electrodes surface. In fact, at the end of experiment the cells were opened, and a well-distributed and adhered bacteria biofilm was observed in the C-SADDLES anode (see Figure S2a in the SI); conversely, in the C-FELT material the precipitation of bacteria and salts at the bottom of anode chamber was evidenced (see Figure S2b in the SI). Based on these results, a higher concentration of bacteria (especially if electroactive), should favor a stable electricity generation, as was observed from the polarization curves (Figure 2) and EIS analysis (reported here below) for the C-SADDLES cell with respect to the C-FELT one.

7
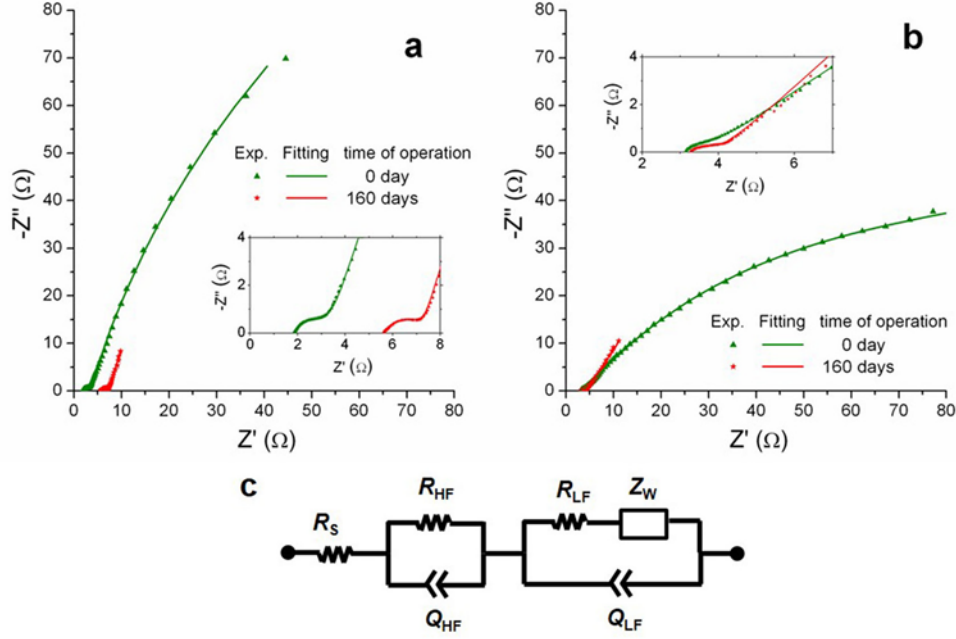
Figure 3. EIS measurements on MFCs during 5 months operation in two-electrode configuration at OCV: (a) carbon felt-based and (b) Berl saddles-based MFCs. The insets show the zoom of the high-frequency region of the curves. (c) Equivalent circuit exploited for the fitting of the experimental data.

3.1.3. Impedance analysis

In Figures 3a and 3b the impedance spectra collected under OCV condition for the two types of cells, during the first day and after 5 months of operation, are reported. Two features can be recognized in the spectra, a high frequency (HF) process (also visible in the zoom reported in the two insets) which is related to the electrons charge-transfer (activation) in both the anodic and cathodic electrodes, and a low frequency (LF) one, accounting for the anodic biofilm mass-transfer limitations (concentration), which contains the diffusion of the organic substrate in the biofilm and the transfer of charges at the biofilm/electrolyte interface; in addition, the distance between the origin of axes and the initial point of the curves represents the series (ohmic) resistance of the device (comprising contact wiring resistance, electrolytes resistances and membrane resistance). For both cells, a valuable decrease of the impedance was noticed after 5 months of operation, in accordance with the improved performances of the devices already discussed above.

In order to quantitatively evaluate the electrochemical performances of the studied MFCs, the measured spectra were fitted through the equivalent circuit proposed in Figure 3c (Dominguez-Benetton et al., 2012), which is directly linked to the scheme reported in Figure 1 and described above in the introduction section. In the equivalent circuit, the ohmic resistance is represented by R_s; the HF processes is modeled through the parallel between the charge-transfer resistance R_{HF} and the constant phase element (CPE) Q_{HF} (associated to the double layer capacitance C_{HF}):

$$C_{HF} = R_{HF}^{\frac{1}{n_{HF}}} Q_{HF}^{\frac{1}{n_{HF}}-1} \tag{1}$$

where n_{HF} is the CPE index, which is related to the interface porosity; the LF process is represented through the parallel $R_{LF}//Q_{LF}$ (with relations equal to the above described HF parameters), and, in some cases, a Warburg element Z_W (Macdonald, 1992) was added to take

8

into account the diffusion of protonated species from the anodic biofilm to the electrolytic media (Jung et al., 2011). The calculated curves are presented in Figures 3a and 3b superimposed to the experimental ones, while the parameters values are summarized in Table 1. There, the time constants τ_{LF} and τ_{LF} were calculated according to the following formulae:

$$\tau_{HF} = C_{HF} R_{HF} \qquad (2)$$

$$\tau_{LF} = C_{LF} R_{LF} \qquad (3)$$

By looking at the table values, it can be observed that after 5 months of operation the R_s of the carbon felt-based cell increases thrice, probably caused by the higher concentration of planktonic microorganisms as confirmed by the OD_{600} measurements (see Section 3.1), which increase the viscosity of the anolyte. As a consequence, the mobility of H^+ ions became also limited by the mass-transport as indicated by the reduction of the diffusion parameter Z_w (from 0.86 to 0.43 $\Omega \cdot s^{0.5}$). Concerning instead the Berl saddles-based MFC cell, the initial R_s value is higher with respect to the carbon felt-based MFC, likely due to a worse contact between the graphite electrode rod and the 3D-packed saddles randomly distributed inside the total anodic volume, if compared to the graphite-felt couple. However, no significant difference can be appreciated after 5 months, in accordance with a more homogeneous distribution of the planktonic bacteria (already observed by the OD_{600} analyses), which most

probably creates a continuous biofilm in both the Berl saddles and graphite rod surfaces that maintains a good electronic transport and does not limit the ionic mobility. Regarding the HF process, its time constant τ_{HF} remains quite constant during all the investigation period for both MFCs, even if the process is one order of magnitude faster in the Berl saddles-based devices. This feature is likely due to the fact that the 3D-packed electrode favors more the electronic charge-transfer than the planar electrode, as witnessed by the reduced capacitance and resistance components (see the corresponding C_{HF} and R_{HF} values in Table 1).

The increase in the bacteria colonization seems to be also responsible for the reduction of the R_{LF} (R_{conc}) after 5 months of operation, independently on the electrode material. In accordance with the LSV results, the Berl saddles-based cell exhibits larger concentration resistance at the initial stage of the analysis; however, at the end of investigation period both values are of the same order of magnitude and the corresponding short circuit current (SCC) values became similar. Accordingly, the time constants decrease along time for both cells, but the variation is larger for the Berl saddles-based MFC. In addition, its τ_{LF} value is larger with respect to the carbon felt-based devices. For the Berl saddles-based cell, in fact, a larger capacitance was obtained, implying a higher growth of microorganisms in this MFC.

Table 1: Fitting results of EIS measurements on MFCs during 5 months operation in two-electrode configuration at OCV.

MFC	Time	R_s (Ω)	C_{HF} (mF)	n_{HF}	R_{HF} (Ω)	τ_{HF} (ms)	C_{LF} (F)	n_{LF}	R_{LF} (Ω)	τ_{LF} (s)
C-FELT	0 day	1.84	3.86	0.74	1.3	5	0.2	0.89	234	46.9
	160 days	5.64	2.89	0.68	1.68	4.87	0.29	1	127.5	36.9
C-SADDLES	0 day	3.09	0.53	0.71	0.68	0.36	1.66	0.58	389.2	645
	160 days	3.27	0.54	0.74	0.64	0.34	0.72	0.73	113.9	81.8

Although this fact gives a beneficial effect by increasing the current density obtained from the bacteria population in the electrode (observed also by a reduced activation resistance, R_{HF}), at the same time it causes an increase in the capacitive effect due to a higher charge accumulation at the electrode/solution interface. The improved bacteria growth for this class of devices can be justified by the higher porosity of the Berl Saddles that can provide high usable contact surface area with high void bed fraction (about 80 %), as also confirmed by the lower value of the roughness factor n_{LF} (see Table 1).

It is worthy to note that at the initial stage the total internal resistance (R_{INT}) is almost represented by the only R_{LF} values (about 99% for both devices), while after 5 months of operation its influence is slightly lower (about 95%), due to the reduction of the mass-transfer polarization resistances and to the slight increases of the charge-transfer polarization and ohmic resistances. Nevertheless, for the whole period of investigation, the LF process represents the rate-limiting step of the MFC operation (as evidenced by the time constants associated to the two polarization processes).

### 3.2. Comparison between cells after 5 months of operation in three-electrode configuration

3.2.1. Polarization curves

The single contribution of anode and cathode electrodes on the MFC performance was examined by placing a reference electrode into each chamber.

Figure 4 shows anode and cathode polarization curves separately for both the MFCs. The anode working potentials started from ~0.55 V (vs. Ag/AgCl) in OCV condition either for carbon felt or Berl Saddles, but moving towards SC, the current output was higher for C-SADDLES MFC than C-FELT one, thus confirming an easier transfer of electrons to the electrode. Therefore, the anode material and the attached biofim were

the major factors influencing anode features: C-SADDLES, offering a large area for microbes, contribute to the higher quantity of electricity generated.

Instead, looking to the cathode potential, we can confirm that it does not correlate with the anode material. Similar behaviours were found by Sun et al. (Sun et al., 2011). Moreover, since the cathode had a maximum SCC of 90 and 140 $\mu A \cdot cm^{-2}$ for the felt and Berl saddles MFCs, respectively (roughly four-times larger than the anodic values), it was evident that the rate-limiting component of the MFC was the anode oxidation reaction that is mediated by microorganisms. Regarding the reduction reaction, there are different cathodic electron acceptors, such as dissolved oxygen, ferricyanide, potassium permanganate, or manganese dioxide, that have been studied in two-chamber MFCs (Wei et al., 2012). For abiotic cathodes immersed in electrolyte solutions, the electrode reactions of MFCs are heterogeneous and take place in the interfacial region between the solid electrode and the solution (Zhao et al., 2009). In particular, potassium ferricyanide catholyte is one of the most widely used electron acceptors, even if present some disadvantage especially when the size of the reactor increases (Zhang et al., 2015; Zhang et al., 2014).
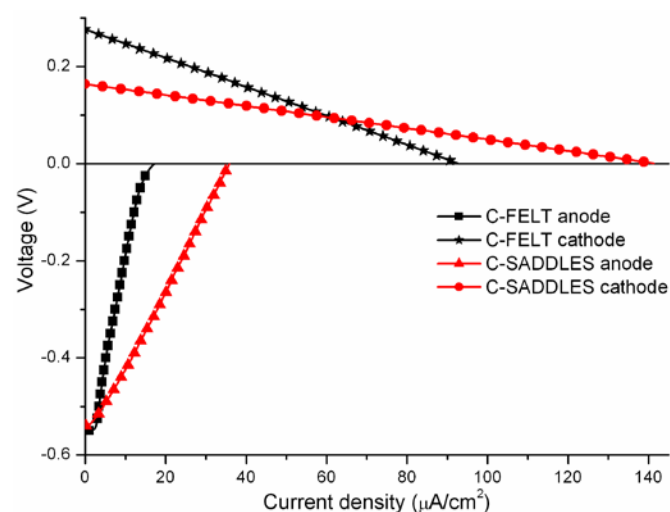
3.2.2. Impedance analysis

Due to the different shapes of the polarization curves of the two kinds of MFC (especially in the case of the Berl saddles-based one) and to the difficulty in understanding the contributions of activation and mass-transfer overpotentials (Logan et al., 2006), we decided to measure and analyze the cell impedances using a three-electrode configuration (as described in the experimental section). In this way, the anodic and cathodic contributions were evaluated separately. In addition, the characterization was repeated for different applied bias voltages, from OCV to SC conditions. The results of the measurements are reported in Figure 5a and 5b, together with the curves obtained by fitting the experimental data with the equivalent circuits shown in Figures 5c (anode) and 5d (cathode).

Concerning the anode compartment, the HF process is associated with the mechanism of charge-transfer at the anode-electrode/biofilm interface (activation resistance), while the LF process is associated with the biofilm/electrolyte interface (mass-transfer resistance). The diffusional Warburg element (Z_w) was considered, when its contribution was observed in the EIS curve. At the cathode, instead, only a charge-transfer polarization process at the cathode-electrode/electrolyte interface is present (as evident in the insets of Figure 5a and 5b, where only a semicircle is visible in the Nyquist plots): as a consequence, only a $R_{HF}//Q_{HF}$ parallel was employed for the modeling. In addition, in both compartments, a series resistance was added to take into account the ohmic resistance due to wiring, membrane and electrolyte (anolyte or catholyte) solution. The parameters evaluated through the fitting procedure are summarized in Tables 2 and 3 for both the carbon felt- and Berl saddles-based MFCs, respectively.

Generally speaking, by reducing the cell potential from OCV to SC, the R_{LF} values

decrease, due to the increase in the current flow. This is explained by the fastening of the rate of conversion of the substrate by the microorganisms, which traduces in a faster electronic transport in the electrolyte/biofilm interface (*i.e.* a lower τ_{LF}). Its impact on the total internal resistance is thus reduced from about 99% at OCV (for both cells) down to either 89% for the C-FELT or 95% for the C-SADDLES, at short circuit conditions. By comparing the other LF parameters (C_{LF} and τ_{LF}) of the two cells, larger values were associated with the Berl saddles-based cell, most likely due to the higher growth of microorganisms in this cell as explained below. Concerning the Warburg impedance, its contribution starts to be significant for lower potentials, *i.e.* in the high current regime, in accordance to what reported by Jung and co-workers (Jung et al., 2011).

Concerning the high-frequency process, both the activation resistance (R_{HF}) and the related time-constant τ_{HF} are one order of magnitude lower by using the Berl saddles-based anode than with the carbon felt one. This is in agreement with the previously reported results in the two-electrode EIS measurements, confirming also the fact that the electronic transfer at the electrode/biofilm interface is more favored in the 3D-packed electrode than in the planar carbon felt material. Similarly, microbial anodes modified with highly conductive materials (*i.e.* carbon nanotubes (CNT), conductive polymer composites, or both) that have been characterized by EIS, revealed only a variation on the charge-transfer resistance, which is usually associated with the inverse of the of the electrochemical reaction rate (Dominguez-Benetton et al., 2012; Qiao et al., 2010; Zou et al., 2008). For instance, functionalization of carbon-based electrodes with CNT, polyaniline (PANI) and more strongly with CNT-PANI composites produced an enhanced charge-transfer rate (reduced R_{HF}) mainly due to an increase in the specific surface-area of the electrode (Dominguez-Benetton et al., 2012; Qiao et al., 2007; Zou et al., 2008). In addition, the τ_{HF}

value remains of the same order of magnitude by varying the potential (and the current flow), which means that the electronic transfer between either
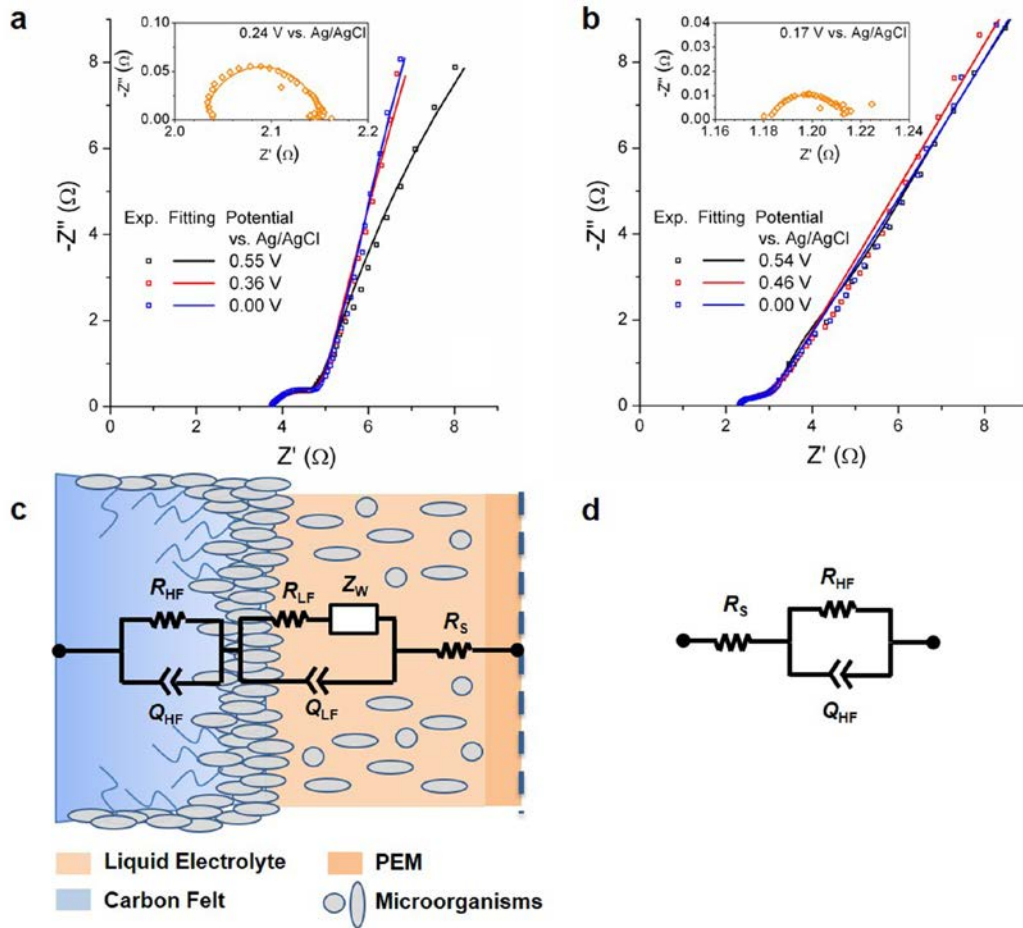
Figure 5. EIS measurements on MFCs anodes after 5 months operation in three-electrode configuration at various potentials: (a) carbon felt-based and (b) Berl saddles-based MFCs. The insets show the corresponding cathode impedance measured at OCV. (c) and (d): equivalent circuits exploited for the fitting of the experimental data of the anode and cathode compartments, respectively.

Table 2: Fitting results of EIS measurements on carbon felt-based MFC after 5 months of operation by using three-electrode configuration, with both anode and cathode used as working electrodes at various potentials.

Working electrode	Potential (V)	R_s (Ω)	C_{HF} (mF)	n_{HF}	R_{HF} (Ω)	τ_{HF} (ms)	C_{LF} (F)	n_{LF}	R_{LF} (Ω)	τ_{LF} (s)
	0.55 (OCV)	3.76	3.49	0.7	1.24	4.33	0.397	0.84	314.8	125
Anode	0.36	3.74	3.87	0.66	1.16	4.46	0.218	0.95	84.6	18.5
	0	3.74	3.28	0.7	0.96	3.15	0.247	0.89	38.9	9.6
Cathode	0.24 (OCV)	2.03	48.8	0.96	0.12	5.7	-	-	-	-

Table 3: Fitting results of EIS measurements on Berl saddles-based MFC after 5 months of operation by using three-electrode configuration, with both anode and cathode used as working electrodes at various potentials.

Working electrode	Potential (V)	R_s (Ω)	C_{HF} (mF)	n_{HF}	R_{HF} (Ω)	τ_{HF} (ms)	C_{LF} (F)	n_{LF}	R_{LF} (Ω)	τ_{LF} (s)
	0.54 (OCV)	2.31	0.47	0.65	0.63	0.29	0.92	0.68	675.2	620
Anode	0.46	2.31	0.45	0.66	0.62	0.28	0.45	0.66	280.5	125
	0	2.38	0.52	0.6	0.7	0.36	0.17	0.77	92	15.9
Cathode	0.17 (OCV)	1.18	46.7	0.66	0.03	1.65	-	-	-	-

the biofilm (at the anode) or the hexacyanoferrate (at the cathode) and the polarized electrodes is faster enough to be sustained under different operative (*i.e.* power density) conditions. With regard to this point, we have to highlight that at the cathodic compartment only one charge-transfer process was found to occur, *i.e.* from the electrode to the electrolytic solution (see insets of Figures 5a and 5b), and that this process is not dependent on the applied bias voltage. It is worth of notice that the electronic transfer at the anode is faster than at the cathode ($\tau_{HF,anode} < \tau_{HF,cathode}$). This implies that the charge-transfer between the biofilm and either the carbon felt- or the Berl saddles-based electrodes is not the rate limiting step in this seawater microorganisms-based MFC systems.

4. Conclusions

A mixed seawater-based microbial population was used as biofilm in the anodic chambers of two MFCs, employing a 2D carbon felt reference electrode and an innovative 3D carbon-coated Berl saddles-based electrode. The electrochemical behavior of the C-FELT cell suffered a decrease of the MPP, while the C-SADDLES MFC maintained constant performances.

Results from EIS analysis confirmed an enhanced charge-transfer in the 3D electrode, due to its high contact surface area, which induced an increase in the bacteria growth, producing a higher power density. The main contribution to the internal resistance was attributed to mass-transport limitations at the biofilm/electrolyte interface.

5. References

Aelterman, P., Versichele, M., Marzorati, M., Boon, N., Verstraete, W. 2008. Loading rate and external resistance control the electricity generation of microbial fuel cells with different three-dimensional anodes. *Bioresource Technology*, **99**(18), 8895-8902.

Arends, J., Desloover, J., Puig, S., Verstraete, W. 2012. Principles and Technology of Microbial Fuel Cells. *Fuel Cell Science and Engineering: Materials, Processes, Systems and Technology*, 147-184.

Barsoukov, E., Macdonald, J.R. 2005. *Impedance spectroscopy: theory, experiment, and applications*. John Wiley & Sons.

Bond, D.R., Strycharz-Glaven, S.M., Tender, L.M., Torres, C.I. 2012. On Electron Transport through Geobacter Biofilms. *ChemSusChem*, **5**(6), 1099-1105.

Clauwaert, P., Aelterman, P., De Schamphelaire, L., Carballa, M., Rabaey, K., Verstraete, W. 2008. Minimizing losses in bio-electrochemical systems: the road to applications. *Applied Microbiology and Biotechnology*, **79**(6), 901-913.

Di Lorenzo, M., Scott, K., Curtis, T.P., Head, I.M. 2010. Effect of increasing anode surface area on the performance of a single chamber microbial fuel cell. *Chemical Engineering Journal*, **156**(1), 40-48.

Dominguez-Benetton, X., Sevda, S., Vanbroekhoven, K., Pant, D. 2012. The accurate use of impedance analysis for the study of microbial electrochemical systems. *Chemical Society Reviews*, **41**(21), 7228-7246.

Du, Z., Li, H., Gu, T. 2007. A state of the art review on microbial fuel cells: a promising technology for wastewater treatment and bioenergy. *Biotechnology advances*, **25**(5), 464-482.

He, Z., Mansfeld, F. 2009. Exploring the use of electrochemical impedance spectroscopy (EIS) in microbial fuel cell studies. *Energy & Environmental Science*, **2**(2), 215-219.

Hernández, S., Cauda, V., Chiodoni, A., Dallorto, S., Sacco, A., Hidalgo, D., Celasco, E., Pirri, C.F. 2014. Optimization of 1D ZnO@ TiO2 Core–Shell Nanostructures for Enhanced Photoelectrochemical Water Splitting under Solar Light Illumination. *ACS applied materials & interfaces*, **6**(15), 12153-12167.

Hernández, S., Hidalgo, D., Sacco, A., Chiodoni, A., Lamberti, A., Cauda, V., Tresso, E., Saracco, G. 2015. Comparison of photocatalytic and transport properties of TiO2

and ZnO nanostructures for solar-driven water splitting. *Physical Chemistry Chemical Physics*, **17**(12), 7775-7786.

Hidalgo, D., Tommasi, T., Cauda, V., Porro, S., Chiodoni, A., Bejtka, K., Ruggeri, B. 2014. Streamlining of commercial Berl saddles: A new material to improve the performance of microbial fuel cells. *Energy*, **71**, 615-623.

Jung, S., Mench, M.M., Regan, J.M. 2011. Impedance characteristics and polarization behavior of a microbial fuel cell in response to short-term changes in medium pH. *Environmental science & technology*, **45**(20), 9069-9074.

Logan, B.E., Hamelers, B., Rozendal, R., Schröder, U., Keller, J., Freguia, S., Aelterman, P., Verstraete, W., Rabaey, K. 2006. Microbial fuel cells: methodology and technology. *Environmental science & technology*, **40**(17), 5181-5192.

Macdonald, J.R. 1992. Impedance spectroscopy. *Annals of Biomedical Engineering*, **20**(3), 289-305.

Manohar, A.K., Bretschger, O., Nealson, K.H., Mansfeld, F. 2008. The use of electrochemical impedance spectroscopy (EIS) in the evaluation of the electrochemical properties of a microbial fuel cell. *Bioelectrochemistry*, **72**(2), 149-154.

Manohar, A.K., Mansfeld, F. 2009. The internal resistance of a microbial fuel cell and its dependence on cell design and operating conditions. *Electrochimica Acta*, **54**(6), 1664-1670.

Martin, E., Savadogo, O., Guiot, S.R., Tartakovsky, B. 2013. Electrochemical characterization of anodic biofilm development in a microbial fuel cell. *Journal of Applied Electrochemistry*, **43**(5), 533-540.

Qiao, Y., Bao, S.-J., Li, C.M. 2010. Electrocatalysis in microbial fuel cells—from electrode material to direct electrochemistry. *Energy & Environmental Science*, **3**(5), 544-553.

Qiao, Y., Li, C.M., Bao, S.-J., Bao, Q.-L. 2007. Carbon nanotube/polyaniline composite as anode material for microbial fuel cells. *Journal of Power Sources*, **170**(1), 79-84.

Sanchez-Herrera, D., Pacheco-Catalan, D., Valdez-Ojeda, R., Canto-Canche, B., Dominguez-Benetton, X., Domínguez-Maldonado, J., Alzate-Gaviria, L. 2014. Characterization of anode and anolyte community growth and the impact of impedance in a microbial fuel cell. *BMC biotechnology*, **14**(1), 102.

Sun, Y., Wei, J., Liang, P., Huang, X. 2011. Electricity generation and microbial community changes in microbial fuel cells packed with different anodic materials. *Bioresource Technology*, **102**(23), 10886-10891.

Tommasi, T., Sassi, G., Ruggeri, B. 2008. Acid pre-treatment of sewage anaerobic sludge to increase hydrogen producing bacteria HPB: effectiveness and reproducibility. *Water Science and Technology*, **58**(8), 1623-1628.

Wei, L., Han, H., Shen, J. 2012. Effects of cathodic electron acceptors and potassium ferricyanide concentrations on the performance of microbial fuel cell. *International journal of hydrogen energy*, **37**(17), 12980-12986.

Yu, Z., Peng, L., Wang, X.-B., Sun, Y.-P. 2012. Influence of initial biofilm growth on electrochemical behavior in dual-chambered mediator microbial fuel cell. *Journal of Fuel Chemistry and Technology*, **40**(8), 967-972.

Zhang, X., Li, K., Yan, P., Liu, Z., Pu, L. 2015. N-type Cu 2 O doped activated carbon as catalyst for improving power generation of air cathode microbial fuel cells. *Bioresource Technology*, **187**, 299-304.

Zhang, Y., Wang, X., Li, X., Gao, N., Wan, L., Feng, C., Zhou, Q. 2014. A novel and high performance activated carbon air-cathode with decreased volume density and catalyst layer invasion for microbial fuel cells. *RSC Advances*, **4**(80), 42577-42580.

Zhao, F., Slade, R.C., Varcoe, J.R. 2009. Techniques for the study and development of microbial fuel cells: an electrochemical

perspective. *Chemical Society Reviews*, **38**(7), 1926-1939.

Zou, Y., Xiang, C., Yang, L., Sun, L.-X., Xu, F., Cao, Z. 2008. A mediatorless microbial fuel cell using polypyrrole coated carbon nanotubes composite as anode material. *International journal of hydrogen energy*, **33**(18), 4856-4862.